CHEMISTRY OF MATERIALS

pubs.acs.org/cm

Article

Stromataxic Stabilization of a Metastable Layered $ScFeO_3$ Polymorph

Lauren M. Garten,*,▽ Zhen Jiang,▽ Hanjong Paik, John D. Perkins, Arvin Kakekhani, Ruixiang Fei, Don J. Werder, Megan E. Holtz, David S. Ginley, Andrew M. Rappe, Darrell G. Schlom, and Margo L. Staruch

Cite This: *Chem. Mater.* 2021, 33, 7423−7431

Read Online

ACCESS | Metrics & More | Article Recommendations | Supporting Information

ABSTRACT: Metastable polymorphs—materials with the same stoichiometry as the ground state but a different crystal structure—enable many critical technologies. This work describes the development of a stabilization approach for metastable polymorphs that are difficult to achieve through other stabilization techniques (such as epitaxy or quenching) called stromataxy. Stromataxy is a method based on controlling the precursor structure during the initial stages of material growth to dictate phase formation. To illustrate this approach, we controlled the atomic layering of the precursors of $ScFeO_3$ and stabilized the metastable $P6_3cm$ phase, under conditions that previously led to the ground-state $Ia\bar{3}$ bixbyite phase. Ab initio mechanistic calculations highlight the importance of the variable oxidation state of Fe and the layer stability during layer-by-layer growth. The broad applicability of a stromataxy approach was demonstrated by stabilizing this metastable phase on substrates that have previously been shown to stabilize other polymorphs under continuous growth. Stromataxy is shown as a viable option for accessing polymorphs that are close in energy, difficult to differentiate by strain, or that lack a well epitaxially matched substrate.

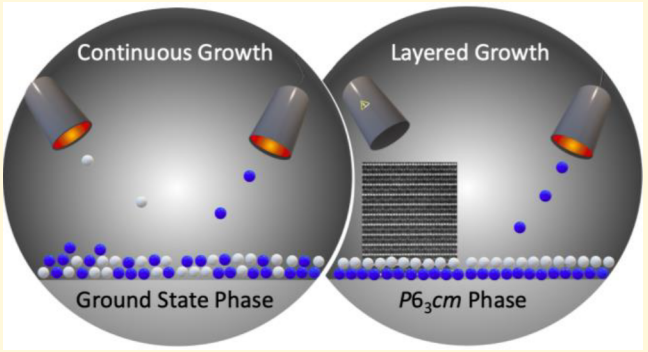

INTRODUCTION

Layered deposition is often used to create layered ceramic compounds;[1−3] it is far more unusual if the grown layered material is metastable but deposited under conditions that previously led to the ground-state phase without layering. So how does changing the deposited structure change which phases could be stabilized? There is well-established precedent for the influence of precursor structure on the morphology and crystallographic texture of the ground-state phase in biology, geology, and materials science.[4−6] For example, it has been shown in some transition-metal oxides that varying the deposition rate leads to the formation of different polymorphs, presumably due to changes in the local structure prior to crystallization.[7−9] Metastable phases have been stabilized by engineering the entropy or enthalpy of alloyed systems, but this route is not viable for less-complex chemistries.[10,11] Perhaps a metastable phase could be stabilized if the temperature is low enough or quenched quickly enough, so that the as-deposited structure could have remnant metastability, similar to what has been done in the shuttered layer-by-layer growth of Ruddlesden−Popper phases.[12−14] But when the temperature is high enough to induce diffusion in similar compounds[15] as well as absorption-controlled growth,[16] as in the present work (where the substrate temperature was kept above 750 °C), remnant capture cannot entirely account for the difference in phase formation pathways.

While there are many well-documented studies on the impact of topotaxy[17,18] (reaction in which the initial crystalline material determines the orientation of the product crystal), there is not an analogous concept for the influence of the initial deposited structures (created before or during the induction of crystallization) on phase formation. In order to solidify this concept and begin the discussion of the underlying methodology behind engineering processing routes, we adopt the term "stromataxy". *Stromataxy* is defined as controlling the structure of the material prior to crystallization (through precursor selection or deposition timing) in order to direct the phase formation pathway. A stromataxic approach can be used when the following conditions are met:

Received: June 17, 2021
Revised: August 28, 2021
Published: September 13, 2021

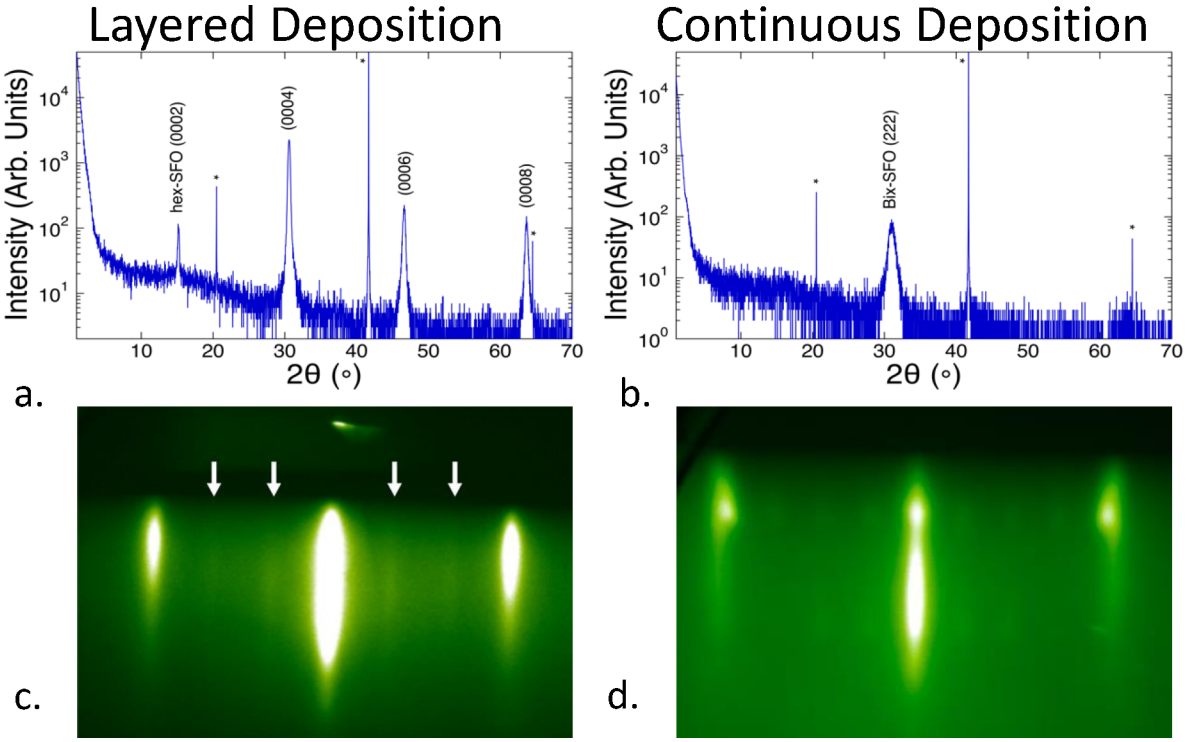

Figure 1. (a) X-ray diffraction (XRD) pattern of a $ScFeO_3$ thin film deposited in discrete alternating layers of scandium and iron onto a (0001) Al_2O_3 sapphire substrate. All peaks fit to the (0001) hexagonal $P6_3cm$ structure. Stars indicate the sapphire peaks. (b) XRD pattern of a $ScFeO_3$ thin film deposited by continuous deposition onto a (0001) Al_2O_3 sapphire substrate, with all other variables held constant. The data are fit to a (222) oriented bixbyite $Ia\bar{3}$ phase. (c) Reflection high-energy electron diffraction (RHEED) taken during layered film growth along the [1000] direction. The arrows highlight the structural features consistent with the scandium distortion in the $P6_3cm$ structure. (d) RHEED taken during continuous film growth indicating a polycrystalline bixbyite phase.

(1) There must be a structural relationship and low-energy pathway between how the precursors (atoms, molecules, or compounds) are assembled during the initial stages of growth and the targeted metastable material. The ground state cannot have features that are too similar energetically and structurally to those of the target metastable polymorph. For example, we show that, while it is possible for the ground-state bixbyite $ScFeO_3$ to be layered (because the scandium and iron are randomly dispersed on a sublattice),[19] it is energetically prohibited.

(2) There is a means of isolating discrete structurally (or energetically) similar elements, either spatially or temporally, to control the precursor structure. In this work, the structural relationship comes from the control of layering, but this could also mean maintaining coordination or morphology from a precursor.[20]

(3) The structure created during deposition should be in an energetic well that is deep enough that it does not relax or diffuse back to the ground state. In the case of the layered $P6_3cm$ $ScFeO_3$, our calculations show that the variable oxidation state and the coordination of the iron layers helps to stabilize the system against diffusion.

(4) For thin films, even though a stromataxic approach does not require dependency on a particular substrate, the substrate can still be used to stabilize the formation of the desired structure needed to promote the targeted metastable phase as the surface of the Al_2O_3 does in the case of metastable $P6_3cm$ $ScFeO_3$.

Previous work has shown the viability of using a stromataxic approach to stabilize metastable multiferroics,[21] layered superconductors,[22] and Ruddlesden−Popper phases by varying the chemistry by layer (i.e., $SrO-SrO-TiO_2$ layers in $Sr_{n+1}Ti_nO_{3n+1}$),[23] but here the selection is between polymorphs with the same fixed stoichiometry. The goal of this work is to investigate the influence of the structuring during growth on the stabilization of phases, in order to be able to develop engineering strategies to target metastable materials. The hexagonal $P6_3cm$ phase of $ScFeO_3$ provides an ideal model system, because it is synthetically accessible[24,25] but still difficult to stabilize, because of the lack of epitaxial substrates and the competition between polymorphs with similar structure and energy.[24,26] Not only is the $P6_3cm$ phase challenging to stabilize, it is also functionally interesting, because of the predicted magnetic properties,[27] measured ferroelectricity,[24] and the precedence of multiferroicity in other polymorphs of $ScFeO_3$[26] and other isostructural materials such as $(Lu,Sc)FeO_3$.[28−30] Here, each of the steps outlined above is discussed in order to develop a stromataxic growth approach.

EXPERIMENTAL METHODS

Film Deposition. $ScFeO_3$ thin films were deposited by molecular beam epitaxy (Veeco Gen10 system) onto (0001) Al_2O_3 substrates (CrysTec, GmbH) for structural and optical measurements. The substrates were cleaned in acetone, IPA, then rinsed in deionized (DI) water. After cleaning, it was annealed in a furnace for 3 h at 1300 °C before loading in the MBE chamber. The back side of substrates were coated with Pt to absorb the radiation heat from the SiC heater. The substrates were kept at ∼750 °C during the deposition. The calibrated Sc flux was 1.9×10^{13} atoms/cm^2 s and Fe flux was 3.8×10^{13} atoms/cm^2 s, respectively. For the layered films, a shuttered growth approach was used, starting with a scandium oxide layer for 48.0 s, then iron oxide at 27.7 s. The background pressure during deposition was $\sim 1 \times 10^{-6}$

https://doi.org/10.1021/acs.chemmater.1c02079
Chem. Mater. 2021, 33, 7423−7431

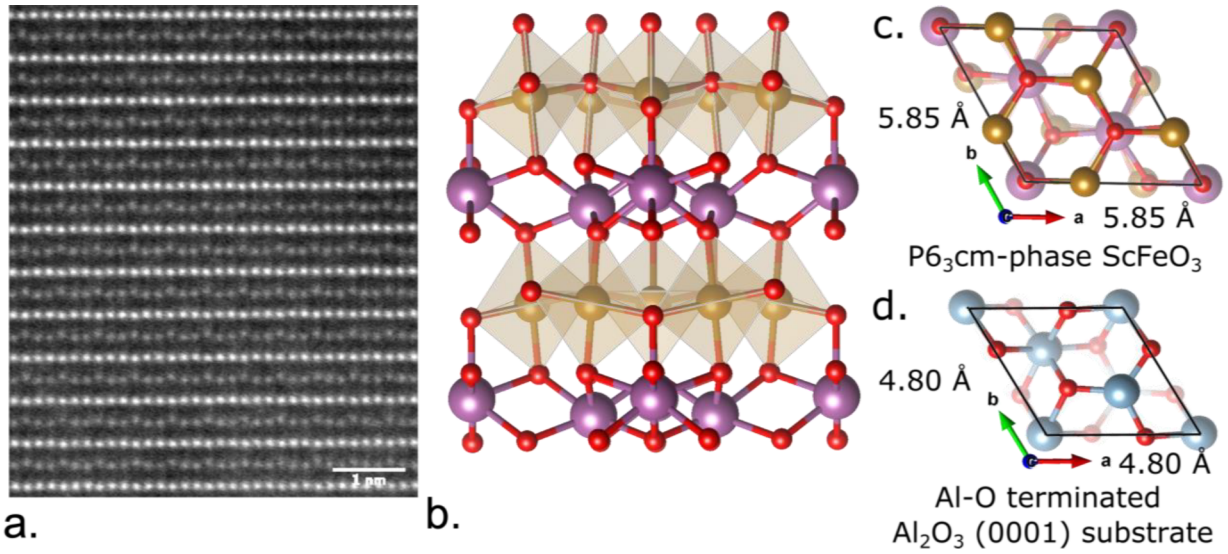

Figure 2. (a) Scanning transmission electron microscopy of a layered $P6_3cm$ $ScFeO_3$ film (scale bar = 1 nm). (b) Schematic of the theory derived unit cell for the layered hexagonal $P6_3cm$ structure [purple, Sc; tan, Fe; and red, O]. (c) (a–b) basal plane projection of the theory-derived unit cell for (0001)-oriented $P6_3cm$ $ScFeO_3$. (d) (a–b) basal plane projection of the theory-derived unit cell for (0001)-oriented Al_2O_3 sapphire substrate.

Torr of 10% ozone with 90% oxygen. The film growth rate and phase were monitored by *in*-situ RHEED, reflective high energy electron diffraction (STAIB Instruments). Further information on the Rutherford backscattering response of the films can be found in the Supporting Information.

X-ray Diffraction. The film structures were determined by X-ray diffraction (XRD). An X-ray diffractometer (Empyrean, Malvern Panalytical) was used to measure the θ–θ, rocking curves, reciprocal space mapping, and phi scans. The X-ray source was Cu Kα radiation (λ = 1.5406 Å).

STEM Imaging. TEM samples were prepared using Thermo Fisher Strata 400 FIB and Helios G4 FIB. Samples were finished at 5KV, 62pA. HAADF STEM images were acquired using a Thermo Fisher Titan Themis S/TEM operating at 300 kV, with a convergence angle of 26 mrad. The final HAADF image was obtained by the image registration[13] of 50 fast (frame time = 0.63 s) images.

Theory. All first-principles studies are computed with plane wave basis sets implemented in the QUANTUM ESPRESSO package.[31] Ultrasoft pseudopotentials[32] and Perdew, Burke, Ernzerhof (PBE) exchange correlations (XC)[33] have been used. Dispersion interactions are taken into account by using the Grimme DFT-D3 method.[34] The DFT+U method[35−37] is applied for the Fe atom, and U = 4.0 eV is chosen.[38] The ferromagnetic moment calculations were performed on the $P6_3cm$-phase $ScFeO_3$, obtaining 3.79°μ_B per Fe atom. The kinetic-energy cutoff for wave functions (E_{cut}) is set at 1090 and 816 eV for Models I and II, respectively, with the charge cutoff being 10 times larger. The sampling of Monkhorst−Pack k-point meshes for the unit cell of $P6_3cm$-phase $ScFeO_3$ and Al_2O_3 is equivalent to 4 × 4 × 2 and 6 × 6 × 2, respectively. The unit cell of layer-ordered bixbyite phase of $ScFeO_3$ was calculated as antiferromagnetic and a k-space mesh of 2 × 2 × 2. Further information on the theory calculations can be found in the Supporting Information.

RESULTS

The impact of stromataxy on phase formation in $ScFeO_3$ is investigated using two different deposition patterns: (1) a continuous flux from both the iron and scandium sources; and (2) alternating flux from only one source at a time, beginning with the scandium layer. The substrate temperature, total pressure, the pressure of O_2, thickness, and stoichiometry are kept constant for these depositions. Further information on the growth conditions is provided in the Methods section. The shutter timing for each layer was determined from the reflection high-energy electron diffraction (RHEED) oscillations during growth. The stoichiometries of both the layered and continuous films were found to be $Sc_1Fe_{1.05}O_3$ by Rutherford backscattering (RBS) (see Figures S1a and S1b in the Supporting Information).

Figure 1a and 1b show the XRD patterns for $ScFeO_3$ films deposited on (0001) sapphire substrates by layered or continuous deposition. Because sapphire substrates do not provide a low-strain epitaxial match for either the $P6_3cm$ phase (16.8% strain, 0001 ‖ 0001) or the $Ia\bar{3}$ phase (10.3% strain, 222 ‖ 0001), the ground-state $Ia\bar{3}$ bixbyite phase[19] would be expected for both processing routes. Bixbyite—the expected ground state for $ScFeO_3$ and Sc_2O_3—is an anion-deficient fluorite-type structure (see Figure S2a in the Supporting Information). The XRD results for a scandium oxide deposition on 111(YSZ), with all other variables held constant, are shown in Figure S2b. In this structure, the Sc and Fe are each 6-fold coordinated by O and randomly distributed on the same sublattice.[19] The diffraction pattern for the continuous films fit to the $Ia\bar{3}$ bixbyite with a (222) orientation. But when grown with alternating flux, the films yield diffraction patterns that can be assigned to the (0001) hexagonal $P6_3cm$ structure instead. This phase has alternating planes: a plane with corner-sharing FeO_5 trigonal bipyramids, and a plane with ScO_7-modified octahedra. The films are phase pure, according to XRD. The hexagonal phase could be grown using continuous growth as a mixture with the ground state, but only for compositions exceeding 12% excess iron (XRD and RBS in Figures S3 and S4 in the Supporting Information). The XRD data are further corroborated by RHEED analyses performed during film growth. In Figure 1c, the white arrows highlight reflections that are unique for the $P6_3cm$ phase and consistent with the with the scandium distortion in this phase. A clear relaxation is seen within the initial layers of growth for both the layered and continuous films. The RHEED pattern observed for the alternating-growth films is clearly distinct from the ground-state bixbyite phase seen in the RHEED of the continuously grown films in Figure 1d. Both the XRD and RHEED indicate that changing the deposition timing, and thus the structure of the material as it is being deposited, changed the energy

https://doi.org/10.1021/acs.chemmater.1c02079
Chem. Mater. 2021, 33, 7423−7431

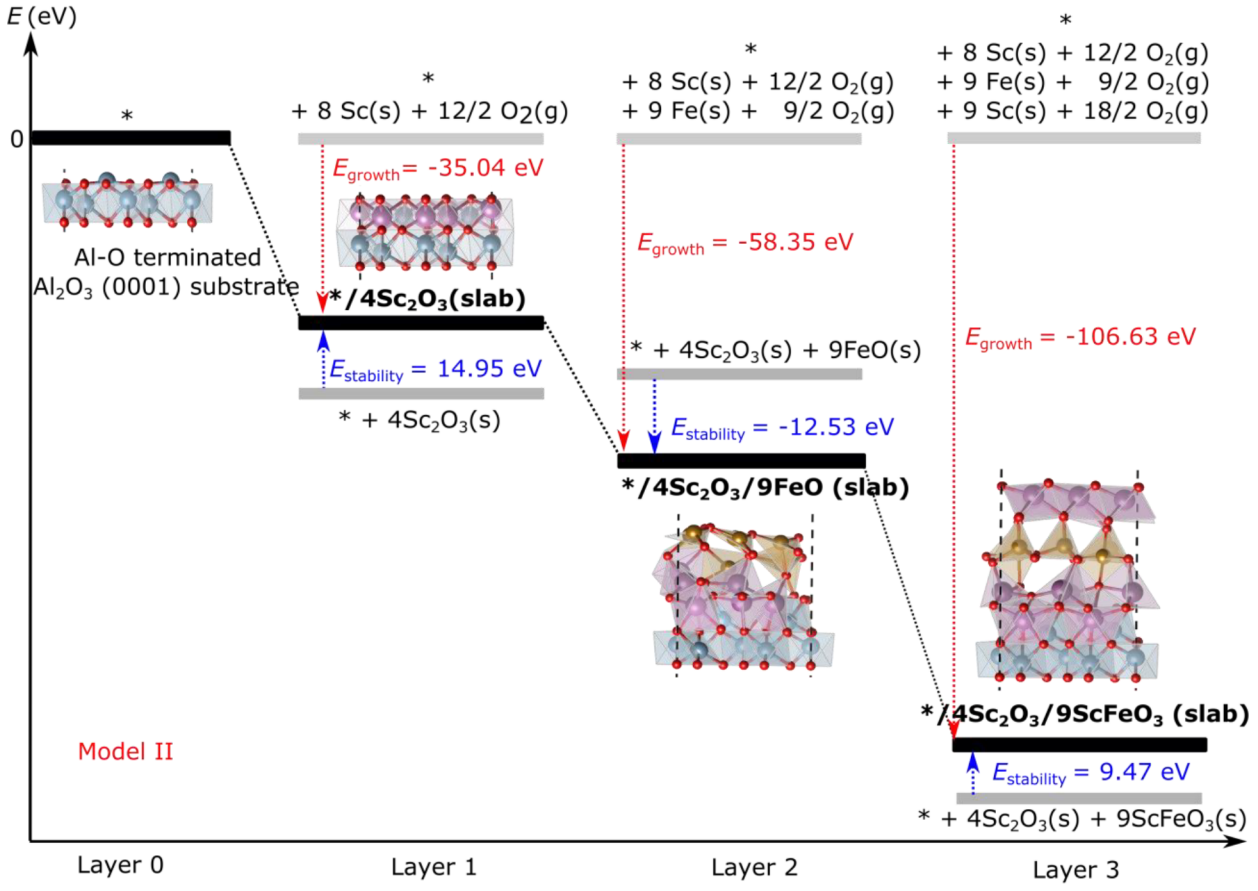

Figure 3. Schematic of the nonepitaxial growth model II in which $\sqrt{3} \times \sqrt{3}\ R30°$ $P6_3cm$-phase $ScFeO_3$ will be grown on the 2 × 2 Al−O-terminated Al_2O_3 (0001) surface. (Model I of the forced epitaxial growth is shown in Figure S6 in the Supporting Information.)

landscape enough to stabilize a metastable phase in stoichiometric films.

The $P6_3cm$ phase is also clearly discernible in the STEM images shown in Figure 2a; the discrete layers of iron and scandium are consistent with the layered hexagonal structure. Alternating growth also appears to mitigate interfacial Fe_3O_4 layers that have previously been observed in $LuFeO_3$ on (111)YSZ.[15] The lattice parameter estimate extracted from the STEM and XRD data, $a = b = 5.85$ Å, $c = 11.60$ Å, $\alpha = \beta = 90°$, $\gamma = 120°$, is consistent with DFT calculations. The structure is analogous to $P6_3cm$ $LuFeO_3$[21] or $EuMnO_3$,[39] where the rotations of FeO_5 trigonal bipyramids in the (0001) plane and the corresponding displacement of the Sc atoms along the [0001] axis, break the inversion symmetry, and form a polar distortion along the [0001] direction. These structural features are highlighted in the schematic of the theory-derived structure in Figure 2b.

In order to understand how precursor structure influences phase formation, the growth process was simulated through ab initio calculations. Two models were explored: Model I was based on forced epitaxy (using an averaged strain state/lattice parameter between the substrate and film of a, b = 5.325 Å); Model II was based on the minimum coincidence lattice of $\sqrt{3} \times \sqrt{3}R30°$ and 2 × 2 unit cells of film and substrate, respectively, for a lattice mismatch of ∼5.5%). The Al−O surface termination of the $(0001)Al_2O_3$ substrate was used because it is the most thermodynamically stable surface at the experimental conditions (T = 1023 K).[40] The basal plane projections of the theory-derived unit cells for $(0001)ScFeO_3$ and $(0001)Al_2O_3$ are shown in Figures 2c and 2d, respectively. The orientation relationship used in each model is shown in Figures S5a and S5b in the Supporting Information. Next, the growth energies (E_{growth}, defined in the Supporting Information) of each Sc and Fe oxide layer were calculated for both +2 and +3 oxidation states. Upon exposure to $Sc+O_2$, the first layer was found to be epitaxial Sc_2O_3 with $E_{growth} = -5.71$ eV per Sc (−4.38 eV per Sc for Model II, see Figure 3). This layer is stabilized by the relaxation of the topmost Al cations into the Sc oxide monolayer at hexagonal Sc sites (instead of Sc at these sites), as shown in Figure 3 for Model II (and in Figure S6 in the Supporting Information for Model I). The position of a supersurface Al is consistent with recent first-principles calculations showing surface piezoelectricity in $Al_2O_3(0001)$.[41] Also, the starting layer has been observed to strongly influence phase stability in similar materials systems in previous studies.[42] (To ensure that the appropriate model is used for the interfacial structure (and, hence, the growth pathway), we calculated different stoichiometries for the initial layers (see Figure S7a in the Supporting Information) and confirmed that the stoichiometry in Figure S6 has more favorable growth energies). The projected density of states (PDOS) analysis of the initial Sc_2O_3 monolayer on top of the Al−O surface shows a strong electronic orbital overlap between Sc and O atoms belonging to both Sc_2O_3 and Al−O layers (see Figure S7b in the Supporting Information). Therefore, the Sc_2O_3 monolayer interacts strongly with the Al_2O_3 surface and can be kinetically stable at the interface (for a certain time before the FeO layer is deposited). The theory findings on the importance of maintaining a uniform Sc_2O_3 monolayer wetting

https://doi.org/10.1021/acs.chemmater.1c02079
Chem. Mater. 2021, 33, 7423−7431

the oxide substrate as a first layer in the growth of $P6_3cm$ $ScFeO_3$ structure is supported by the experimental results showing reduced quality and stability of films grown with an initial Fe layer. The impact of initial Fe deposition on film growth can be seen in the XRD data in Figure S7d in the Supporting Information. Thus, we show that not only does the ordering of layers matter, but also the interaction between the substrate and initial layers can provide stabilization.

After the formation of interfacial Sc_2O_3 layer, $Fe+O_2$ is introduced, leading to the formation of an FeO monolayer (see Figure S7c in the Supporting Information). Next, $Sc+O_2$ react on the surface in a 1:1 ratio, converting the Fe^{2+} to Fe^{3+} and forming a complete $P6_3cm$-phase $ScFeO_3$ layer. Figure 3 (and Figure S6) shows how each layer was built up independently in model II (model I). The growth follows a pathway of substrate* → substrate*(Sc_2O_3) → substrate*(Sc_2O_3)-(FeO) → substrate*(Sc_2O_3)($ScFeO_3$), where the substrate* shares Al−O when (0001) Al_2O_3 is used. Interestingly, the capability of Fe atoms to assume both +2 and +3 oxidation states enables the viability of such a growth mechanism. When the Fe layer is the termination, prior to the deposition of a $Sc+O_2$ capping layer, it only stabilizes a limited number of oxygens, favorably reaching +2 rather than forming the +3 oxidation state of Fe. However, once Fe atoms are in an interior layer, the extended bulk bonding motif provides enough neighboring O atoms for Fe to reach the +3 oxidation state. Layered growth was also found to be energetically favorable in model II. Thus, the stoichiometry of each layer in the growth pathway appears to be robust, regardless of the exact interfacial model.

The next step is to understand the stability of each layer after deposition and its resistance to diffusion or relaxing back to the ground state. The thermodynamic stability of each Sc/Fe-oxide monolayer after deposition was studied by computing the grown slab energy, relative to the Al_2O_3 slab and the bulk oxides ($E_{stability}$, defined in the Supporting Information). Interdiffusion of Sc and Fe in models I and II are shown in Figures S8a and S8b in the Supporting Information, respectively. In both models, $E_{stability}$ reaches almost the same value once a unit cell of stoichiometric $ScFeO_3$ is formed (Layer 3). Because bixbyite, the expected ground state for $ScFeO_3$ and Sc_2O_3, is an anion-deficient fluorite-type structure with scandium and iron randomly distributed on the same sublattice,[7] we also studied the interdiffusion behavior between Sc and Fe oxide monolayers by calculating the swap energy (E_{swap}, defined in the Supporting Information). The interfacial Sc/Fe interdiffusion is found to be thermodynamically favorable only when the second Fe monolayer is the surface termination. Once another Sc-oxide monolayer is deposited above that FeO layer, the interdiffusion of Fe to either the top or bottom scandium layers is disfavored and suppressed. This is counter to what has previously been seen in Ruddlesden−Popper titanates,[43] again suggesting the importance of the variable oxidation state of Fe in this material. To get a more general view of interdiffusion during the growth process, we model diffusion in the bulk $P6_3cm$-phase $ScFeO_3$. The E_{swap} is always thermodynamically uphill (by >0.72 eV), with a large kinetic barrier of ∼5.5 eV (shown in Figure S8c in the Supporting Information). Thus, we obtained a negligible interdiffusion rate of 8×10^{-15} s^{-1} based on the assumption of a pre-exponential factor of $A = 1 \times 10^{13}$ s^{-1} and $T = 1023$ K. We therefore conjecture that once relatively ordered $ScFeO_3$ units form, they are protected against Sc/Fe interdiffusion, regardless of the specific growth substrate.

Finally, we studied the formation preference for metastable $P6_3cm$ phase compared with that of the ground-state bixbyite phase using stromataxic alternating layer-by-layer growth. To emulate the structure of the deposited films, layered bixbyite was investigated instead of a randomly Sc/Fe populated structure with fractional site occupancies (see Figures S9a and S9b in the Supporting Information). A layered bixbyite configuration is energetically unfavorable. While such a polar bonding network (due to large out-of-plane separation between O atoms and the metal cations) is favorable in an extended 3D structure, layer-by-layer growth exposes each layer to a significant amount of undercoordination. Because of the large out-of-plane separation between Fe and O layers (in layered bixbyite), the undercoordinated O layer relaxes inward, toward the FeO layer, forming Sc−O bonds. Thus, the growing film attempting to construct a layered bixbyite leads to a structure that is more similar to the $P6_3cm$ phase. Growth along the (222) direction of layered bixbyite is also considered to match the experimental results (Figure S9C in the Supporting Information). Although such a direction is not as polar, growth of a layered bixbyite structure incurs higher energy penalties. The layered bixbyite's surface energy is ∼1.28 J/m^2, which is considerably larger than 0.87 J/m^2, the surface energy of the metastable $P6_3cm$ phase (see details in the Supporting Information). The higher surface energy is due to more interlayer Sc−O and Fe−O bonds (an average of three interlayer bonds above each cation) in this bixbyite phase, compared with that of $P6_3cm$ phase (1 interlayer bond above each Fe cation, 3−4 interlayer bonds above each Sc). In bixbyite, the Sc and Fe are well-coordinated into octahedra, making it the preferred thermodynamic ground state. The $P6_3cm$ phase is slightly less stable, perhaps due to the 5-fold coordinated Fe triangular bipyramids, but this structure (only one interlayer bond above Fe) makes it more favorable to grow via the layer-by-layer deposition method. In addition to the previous substrate-independent arguments, for the special case of $ScFeO_3$ on the Al-terminated Al_2O_3 (0001), the growth of $P6_3cm$ phase gets a boost due to the fact that the initially deposited Sc_2O_3 monolayer and Al_2O_3 substrate share the same hexagonal structure. Namely, Sc prefers the hollow sites above the surface O atoms on the Al_2O_3 substrate, which is not possible in a structure mimicking the bixbyite phase, in which Sc is located at the bridge or top sites of the sublayer O atoms.

Equipped with a better understanding of the mechanisms behind stromataxic growth, the next step is to determine the general applicability of this layered stromataxy method. Because stabilization comes from the layering in this method and not the substrate-induced strain, layered growth is expected to stabilize the hexagonal phase even on substrates that do not have a close epitaxial fit. To vet this hypothesis, $ScFeO_3$ was deposited via a layered approach on substrates that all have a closer lattice match to one of the five other physically realized $ScFeO_3$ polymorphs.[25] The one-dimensional plot of the a lattice parameters of each of the substrates and polymorphs is presented in Figure S10 in the Supporting Information. The layered deposition results from this work, shown in Table 1, are clearly different from the phases stabilized in previous work using continuous deposition. The hexagonal $P6_3cm$ phase was stabilized on (111) YSZ, (111) Nb:STO, Fe_2O_3/metal/(111) YSZ, (111) $MgAl_2O_4$, and (0001) sapphire. Figures 4a, 4b, and 4c show the XRD confirming the stabilization of the $P6_3cm$ phase on (111) $MgAl_2O_4$, (111) Nb:STO, and (111) YSZ, respectively. The presence of the $P6_3cm$ phase is corroborated by the RHEED, shown in Figures 4 d, 4e, and 4f for the same films.

https://doi.org/10.1021/acs.chemmater.1c02079
Chem. Mater. 2021, 33, 7423−7431

Table 1. Comparison of the Phase Formation of $ScFeO_3$ over a Range of Different Substrates Using Continuous Deposition (Previous Work) and Layered Deposition (This Work)

substrate	previous work	this work
(111) $SrTiO_3$	$Pna2_1$	$P6_3cm$
(111) YSZ	$Ia\bar{3}$	$P6_3cm$
(111) $MgAl_2O_4$	$P6_3cm$	$P6_3cm$
(0001) Al_2O_3	$P6_3cm$	$P6_3cm$
Fe_2O_3/Ir/(111) YSZ	$R\bar{3}c$	$P6_3cm$

The RHEED of films on (111) YSZ show clear 3′1 reconstructions for the hexagonal films.

Growth of the hexagonal phase on (111) YSZ is somewhat surprising, because of (1) the much closer lattice match to the ground state (6.6% mismatch to (222) bixbyite vs. 26.5% (0001) $P6_3cm$); (2) the facile growth of (bixbyite-phase) Sc_2O_3 on (111) YSZ (shown in Figure S2b); and (3) reports of continuous growth on (111) YSZ leading to the ground state.[10] The (111) Nb:$SrTiO_3$ substrates provide the closest one-dimensional epitaxial fit of ∼3.5%. However, the stabilization of hexagonal phase is not assured, because this substrate provides a closer match to another predicted polymorph, the *Pnma* phase. Layered growth on (111) $SrTiO_3$ preferentially stabilized the hexagonal phase, despite previous work that shows the formation of the κ−Al_2O_3 type $Pna2_1$ phase under continuous deposition.[25] In that work, the presence of the κ-Al_2O_3 structure was attributed to the similarities in structure across the substrate film interface. It is also important to note that the reported stoichiometry in the previous work was $Sc_{0.48}Fe_{1.52}O_3$, so this off-stoichiometry could also have played a role in determining the grown phase, similar to what was observed here with films with compositions beyond 10% iron excess. Only films on (001) $SrTiO_3$ did not show the hexagonal phase under alternating-layer growth. However, overall, the range of substrates upon which this *P*63*cm* phase can be grown on using alternating layered growth is extended much further than would be expected solely based on epitaxy.

Demonstrating the success of this growth approach on an array of lattice-mismatched substrates supports the broad applicability of a stromataxic approach. This also indicates that, for some thin-film materials, there are routes to stabilization that can be completely independent of the substrate. It is anticipated that an even wider range of substrates could be used to grow the $P6_3cm$ phase, and similar layered structures, using a stromataxic approach. In addition, the case of the $P6_3cm$ phase on sapphire shows that there are other potential benefits provided by the substrate beyond epitaxy, e.g., the relaxation of the substrate surface into the film, leading to increased stabilization of the initial scandium layers. Substrate selection moving forward should look beyond lattice matching to the benefits of other three-dimensional (3D) structural motifs and larger minimum coincidence lattice matching with the film.

A stromataxic approach could be particularly useful for targeting metastable polymorphs that are similar in energy to other phases or difficult to differentiate from other phases by epitaxial strain, alloying, or quenching. It could also allow for the integration of materials into complex device architectures that would otherwise be prohibitive, because of a lack of lattice-matched substrate, or incompatibility of processing conditions. Furthermore, stromataxy need not be limited to metastable materials or MBE growth.[44,45] For example, growth by atomic layer deposition, where materials are often deposited at low temperature, in discrete layers, from complex precursors, could also be a viable route for the stromataxic stabilization of metastable materials. Similar layered hexagonal and delafossite materials are additional compounds where stromataxy could be an effective means of accessing metastable structures. Ultimately, any structure that can be differentiated by layering

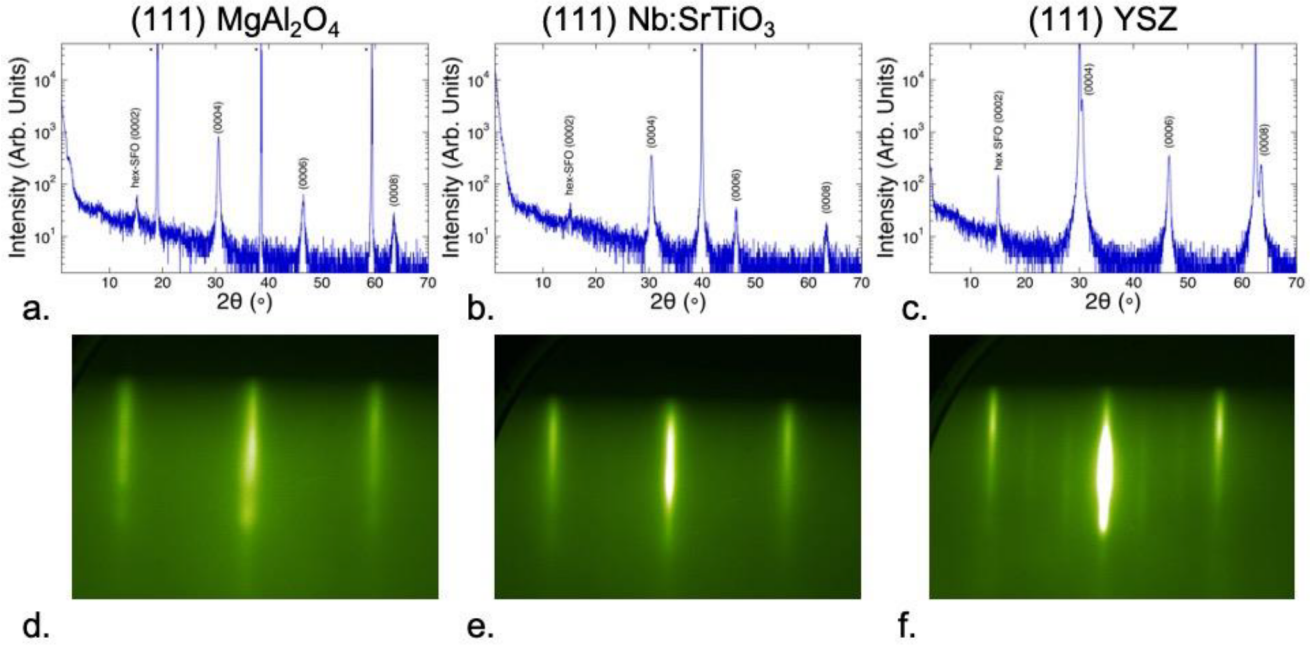

Figure 4. (a−c) XRD of $ScFeO_3$ films grown by layered deposition on (111) $MgAl_2O_4$ substrates (panel (a)), (111) Nb-doped $SrTiO_3$ substrates (panel (b)), and (111) yttria-stabilized zirconia (YSZ) substrates (panel (c)) showing that the hexagonal phase formation is broadly accessible and not unique to a specific substrate. (d−f) RHEED of the same films shown in (111) $MgAl_2O_4$ substrates (panel (d)), (111) Nb-doped $SrTiO_3$ substrates (panel (e)), and (111) yttria-stabilized zirconia (YSZ) substrates (panel (f)).

https://doi.org/10.1021/acs.chemmater.1c02079
Chem. Mater. 2021, 33, 7423−7431

of the precursor geometry, through either deposition energy or timing, could be a candidate for stromataxy.

CONCLUSION

In conclusion, the metastable $P6_3cm$ phase of $ScFeO_3$ was stabilized using a stromataxic approach. Growth via discrete layers stabilizes high-quality, phase-pure $P6_3cm$ phase, while continuous growth creates the ground state for the same chemistry, temperature, pressure, and thickness. The ab initio calculations point to the importance of having a variable oxidation state, and layer stability (related to few dangling bonds) during layer-by-layer growth, for the development of a stromataxic response. These calculations also highlight the importance of the interaction between the substrate and the initial layers of growth in the stabilization of the phase. Using this understanding, a stromataxic approach was engineered and translated across an array of lattice-mismatched substrates, which show the $P6_3cm$ phase when deposited by layered growth but have previously been shown to stabilize other phases in the absence of layering. Overall, stromataxy is shown as a viable option for accessing polymorphs that have similar energies, are difficult to differentiate by strain, or lack a well epitaxially matched substrate.

ASSOCIATED CONTENT

Supporting Information

The Supporting Information is available free of charge at https://pubs.acs.org/doi/10.1021/acs.chemmater.1c02079.

Further theory details; Rutherford backscattering results; ground-state structure and XRD results; DFT model descriptions; diffusion and structural stability models (PDF)

AUTHOR INFORMATION

Corresponding Author

Lauren M. Garten − *Materials Science and Technology Division, U.S. Naval Research Laboratory, Washington, DC 20375, United States; School of Materials Science and Engineering, Georgia Institute of Technology, Atlanta, Georgia 30332, United States;* orcid.org/0000-0002-9482-227X; Email: Lauren.garten@mse.gatech.edu

Authors

Zhen Jiang − *Department of Chemistry, University of Pennsylvania, Philadelphia, Pennsylvania 19104-6323, United States;* orcid.org/0000-0002-1175-5658

Hanjong Paik − *Platform for the Accelerated Realization, Analysis, and Discovery of Interface Materials (PARADIM), Ithaca, New York 14853-1501, United States*

John D. Perkins − *National Renewable Energy Laboratory, Golden,, Colorado 80401, United States;* Present Address: National Institute of Standards and Technology (NIST), Boulder, CO, 80305 (J. D. Perkins)

Arvin Kakekhani − *Department of Chemistry, University of Pennsylvania, Philadelphia, Pennsylvania 19104-6323, United States;* orcid.org/0000-0002-8553-7776

Ruixiang Fei − *Department of Chemistry, University of Pennsylvania, Philadelphia, Pennsylvania 19104-6323, United States*

Don J. Werder − *Platform for the Accelerated Realization, Analysis, and Discovery of Interface Materials (PARADIM), Ithaca, New York 14853-1501, United States*

Megan E. Holtz − *Department of Materials Science and Engineering, Cornell University, Ithaca, New York 14853-1501, United States;* Present Address: Metallurgical & Materials Engineering, Colorado School of Mines, 1301 19th Street Golden, CO 80401 (M. E. Holtz).

David S. Ginley − *National Renewable Energy Laboratory, Golden,, Colorado 80401, United States*

Andrew M. Rappe − *Department of Chemistry, University of Pennsylvania, Philadelphia, Pennsylvania 19104-6323, United States;* orcid.org/0000-0003-4620-6496

Darrell G. Schlom − *Department of Materials Science and Engineering, Cornell University, Ithaca, New York 14853-1501, United States; Kavli Institute at Cornell for Nanoscale Science, Ithaca, New York 14853-1501, United States;* orcid.org/0000-0003-2493-6113

Margo L. Staruch − *Materials Science and Technology Division, U.S. Naval Research Laboratory, Washington, DC 20375, United States*

Complete contact information is available at: https://pubs.acs.org/10.1021/acs.chemmater.1c02079

Author Contributions

$^{\nabla}$These authors made equal contributions.

Author Contributions

L.M.G. and H.P. grew the films with the guidance of M.L.S. and D.G.S.; the XRD and RHEED was taken by L.M.G. and H.P.; J.D.P. measured the RBS; Z.J., A.K., and R.F. formulated the theory and ran calculations under the guidance of A.M.R.; M.E.H. and D.J.W. took and analyzed the STEM; D.G.S., D.S.G., and M.L.S. coordinated the work.

Notes

The authors declare no competing financial interest.

ACKNOWLEDGMENTS

The film synthesis and electron microscopy work was supported by the National Science Foundation (Platform for the Accelerated Realization, Analysis, and Discovery of Interface Materials (PARADIM)), under Cooperative Agreement No. DMR-2039380. This work made use of a Helios FIB supported by NSF (No. DMR-1539918) and the Cornell Center for Materials Research Shared Facilities, which are supported through the NSF MRSEC program (No. DMR-1719875). Z.J. acknowledges support from ARL/ARO via the Collaborative for Hierarchical Agile and Responsive Materials (CHARM), under Cooperative Agreement No. W911NF-19-2-0119. A.K. acknowledges support from the U.S. Department of Energy (DOE), Office of Science, Office of Basic Energy Sciences, under Grant No. DE-SC0019281. R.F. and A.M.R. acknowledge support from the Office of Naval Research, under Grant No. N00014-20-1-2701. The authors acknowledge computational support from the National Energy Research Scientific Computing Center (NERSC) of the DOE and the High-Performance Computing Modernization Office (HPCMO) of the U.S. Department of Defense (DOD). L.M.G. acknowledges the support of the Jerome and Isabella Karle Distinguished Scholar Fellowship from the U.S. Naval Research Laboratory. L.M.G. would like to acknowledge helpful discussions with D. Rowenhorst. D.J.W. acknowledges helpful discussions with Berit Goodge and Lena F. Kourkoutis.

REFERENCES

(1) Lee, J. H.; Luo, G.; Tung, I. C.; Chang, S. H.; Luo, Z.; Malshe, M.; Gadre, M.; Bhattacharya, A.; Nakhmanson, S. M.; Eastman, J. A.; et al. Dynamic Layer Rearrangement during Growth of Layered Oxide Films by Molecular Beam Epitaxy. *Nat. Mater.* **2014**, *13* (9), 879−883.

(2) Cho, A. Y. Growth of Periodic Structures by the Molecular-Beam Method. *Appl. Phys. Lett.* **1971**, *19* (11), 467−468.

(3) Xu, J.; Katoch, J.; Ahmed, A. S.; Pinchuk, I. V.; Young, J. R.; Johnston-Halperin, E.; Pelz, J.; Kawakami, R. K. Growth of Uniform $CaGe_2$ Films by Alternating Layer Molecular Beam Epitaxy. *J. Cryst. Growth* **2017**, *460*, 134−138.

(4) Chen, B. R.; Sun, W.; Kitchaev, D. A.; Mangum, J. S.; Thampy, V.; Garten, L. M.; Ginley, D. S.; Gorman, B. P.; Stone, K. H.; Ceder, G. Understanding Crystallization Pathways Leading to Manganese Oxide Polymorph Formation. *Nat. Commun.* **2018**, *9* (1), 2553.

(5) Smolyar, I.; Bromage, T.; Wikelski, M. Quantification of Layered Patterns with Structural Anisotropy: A Comparison of Biological and Geological Systems. *Heliyon* **2016**, *2* (3), e00079.

(6) Kato, T. Polymer/Calcium Carbonate Layered Thin-Film Composites. *Adv. Mater.* **2000**, *12* (20), 1543−1546.

(7) Stone, K. H.; Schelhas, L. T.; Garten, L. M.; Shyam, B.; Mehta, A.; Ndione, P. F.; Ginley, D. S.; Toney, M. F. Influence of Amorphous Structure on Polymorphism in Vanadia. *APL Mater.* **2016**, *4* (7), 076103.

(8) Mangum, J. S.; Garten, L. M.; Ginley, D. S.; Gorman, B. P. Utilizing TiO_2 Amorphous Precursors for Polymorph Selection: An in Situ TEM Study of Phase Formation and Kinetics. *J. Am. Ceram. Soc.* **2020**, *103* (4), 2899.

(9) Mangum, J. S.; Agirseven, O.; Haggerty, J. E. S.; Perkins, J. D.; Schelhas, L. T.; Kitchaev, D. A.; Garten, L. M.; Ginley, D. S.; Toney, M. F.; Tate, J. Selective Brookite Polymorph Formation Related to the Amorphous Precursor State in TiO_2 Thin Films. *J. Non-Cryst. Solids* **2019**, *505*, 109.

(10) Rost, C. M.; Sachet, E.; Borman, T.; Moballegh, A.; Dickey, E. C.; Hou, D.; Jones, J. L.; Curtarolo, S.; Maria, J. P. Entropy-Stabilized Oxides. *Nat. Commun.* **2015**, *6* (1), 1−8.

(11) Siol, S.; Holder, A.; Steffes, J.; Schelhas, L. T.; Stone, K. H.; Garten, L.; Perkins, J. D.; Parilla, P. A.; Toney, M. F.; Huey, B. D. Negative-Pressure Polymorphs Made by Heterostructural Alloying. *Sci. Adv.* **2018**, *4* (4), eaaq1442.

(12) Maritato, L.; Galdi, A.; Orgiani, P.; Harter, J. W.; Schubert, J.; Shen, K. M.; Schlom, D. G. Layer-by-Layer Shuttered Molecular-Beam Epitaxial Growth of Superconducting $Sr_{1-X}La_xCuO_2$ Thin Films. *J. Appl. Phys.* **2013**, *113* (5), No. 053911.

(13) Yan, L.; Niu, H. J.; Duong, G. V.; Suchomel, M. R.; Bacsa, J.; Chalker, P. R.; Hadermann, J.; van Tendeloo, G.; Rosseinsky, M. J. Cation Ordering within the Perovskite Block of a Six-Layer Ruddlesden-Popper Oxide from Layer-by-Layer Growth - Artificial Interfaces in Complex Unit Cells. *Chem. Sci.* **2011**, *2* (2), 261−272.

(14) Tanaka, H.; Kawai, T. Artificial Construction of SrO/(La,Sr)MnO_3 Layered Perovskite Superlattice by Laser Molecular-Beam Epitaxy. *Appl. Phys. Lett.* **2000**, *76*, 3618.

(15) Akbashev, A. R.; Roddatis, V. V.; Vasiliev, A. L.; Lopatin, S.; Amelichev, V. A.; Kaul, A. R. Reconstruction of the Polar Interface between Hexagonal $LuFeO_3$ and Intergrown Fe_3O_4 Nanolayers. *Sci. Rep.* **2012**, *2*, 672 DOI: 10.1038/srep00672.

(16) Brooks, C. M.; Misra, R.; Mundy, J. A.; Zhang, L. A.; Holinsworth, B. S.; O'Neal, K. R.; Heeg, T.; Zander, W.; Schubert, J.; Musfeldt, J. L.; et al. The Adsorption-Controlled Growth of $LuFe_2O_4$ by Molecular-Beam Epitaxy. *Appl. Phys. Lett.* **2012**, *101* (13), 132907.

(17) Figlarz, M.; Gérand, B.; Delahaye-Vidal, A.; Dumont, B.; Harb, F.; Coucou, A.; Fievet, F. Topotaxy, Nucleation and Growth. *Solid State Ionics* **1990**, *43* (C), 143−170.

(18) Mairoser, T.; Mundy, J. A.; Melville, A.; Hodash, D.; Cueva, P.; Held, R.; Glavic, A.; Schubert, J.; Muller, D. A.; Schlom, D. G. High-Quality EuO Thin Films the Easy Way via Topotactic Transformation. *Nat. Commun.* **2015**, *6*, 7716.

(19) Bréard, Y.; Fjellvag, H.; Hauback, B. Investigation of Bixbyite Type Scandium Oxides Involving a Magnetic Cation: $Sc_{2-x}Fe_xO_3$ ($0 \leq x \leq 1$). *Solid State Commun.* **2011**, *151* (3), 223−226.

(20) Tappan, B. A.; Barim, G.; Kwok, J. C.; Brutchey, R. L. Utilizing Diselenide Precursors toward Rationally Controlled Synthesis of Metastable $CuInSe_2$ Nanocrystals. *Chem. Mater.* **2018**, *30* (16), 5704−5713.

(21) Mundy, J. A.; Brooks, C. M.; Holtz, M. E.; Moyer, J. A.; Das, H.; Rébola, A. F.; Heron, J. T.; Clarkson, J. D.; Disseler, S. M.; Liu, Z.; et al. Atomically Engineered Ferroic Layers Yield a Room-Temperature Magnetoelectric Multiferroic. *Nature* **2016**, *537* (7621), 523−527.

(22) Schlom, D. G.; Eckstein, J. N.; Hellman, E. S.; Streiffer, S. K.; Harris, J. S.; Beasley, M. R.; Bravman, J. C.; Geballe, T. H.; Webb, C.; Von Dessonneck, K. E.; et al. Molecular Beam Epitaxy of Layered Dy-Ba-Cu-O Compounds. *Appl. Phys. Lett.* **1988**, *53* (17), 1660−1662.

(23) Haeni, J. H.; Theis, C. D.; Schlom, D. G.; Tian, W.; Pan, X. Q.; Chang, H.; Takeuchi, I.; Xiang, X.-D. Epitaxial Growth of the First Five Members of the $SrN+1Ti_nO_{3n+1}$ Ruddlesden-Popper Homologous Series. *Appl. Phys. Lett.* **2001**, *78*, 3292.

(24) Hamasaki, Y.; Katayama, T.; Yasui, S.; Shiraishi, T.; Akama, A.; Kiguchi, T.; Taniyama, T.; Itoh, M. Switchable Third $ScFeO_3$ Polar Ferromagnet with $YMnO_3$-Type Structure. *J. Mater. Chem. C* **2020**, *8* (13), 4447−4452.

(25) Hamasaki, Y.; Shimizu, T.; Yasui, S.; Taniyama, T.; Sakata, O.; Itoh, M. Crystal Isomers of $ScFeO_3$. *Cryst. Growth Des.* **2016**, *16* (9), 5214−5222.

(26) Kawamoto, T.; Fujita, K.; Yamada, I.; Matoba, T.; Kim, S. J.; Gao, P.; Pan, X.; Findlay, S. D.; Tassel, C.; Kageyama, H.; et al. Room-Temperature Polar Ferromagnet $ScFeO_3$ Transformed from a High-Pressure Orthorhombic Perovskite Phase. *J. Am. Chem. Soc.* **2014**, *136* (43), 15291−15299.

(27) Sinha, K.; Wang, H.; Wang, X.; Zhou, L.; Yuewei Yin, K.; Wang, H.; Wang, X.; Zhou, L.; Yin, Y.; Wang, W.; Cheng, X.; Keavney, D. J.; Cao, H.; Liu, Y.; et al. Tuning the Néel Temperature of Hexagonal Ferrites by Structural Distortion. *Phys. Rev. Lett.* **2018**, *121*, 237203.

(28) Disseler, S. M.; Borchers, J. A.; Brooks, C. M.; Mundy, J. A.; Moyer, J. A.; Hillsberry, D. A.; Thies, E. L.; Tenne, D. A.; Heron, J.; Holtz, M. E.; et al. Magnetic Structure and Ordering of Multiferroic Hexagonal $LuFeO_3$. *Phys. Rev. Lett.* **2015**, *114* (21), 217602.

(29) Du, K.; Gao, B.; Wang, Y.; Xu, X.; Kim, J.; Hu, R.; Huang, F. T.; Cheong, S. W. Vortex Ferroelectric Domains, Large-Loop Weak Ferromagnetic Domains, and Their Decoupling in Hexagonal (Lu, Sc)FeO_3. *npj Quantum Mater.* **2018**, *3* (1), DOI: 10.1038/s41535-018-0106-3.

(30) Xu, X.; Wang, W. Multiferroic Hexagonal Ferrites (h-$RFeO_3$, R = Y, Dy-Lu): A Brief Experimental Review. *Mod. Phys. Lett. B* **2014**, *28* (21), 1430008.

(31) Giannozzi, P.; Baroni, S.; Bonini, N.; Calandra, M.; Car, R.; Cavazzoni, C.; Ceresoli, D.; Chiarotti, G. L.; Cococcioni, M.; Dabo, I.; et al. QUANTUM ESPRESSO: A Modular and Open-Source Software Project for Quantum Simulations of Materials. *J. Phys.: Condens. Matter* **2009**, *21* (39), 395502.

(32) Garrity, K. F.; Bennett, J. W.; Rabe, K. M.; Vanderbilt, D. Pseudopotentials for High-Throughput DFT Calculations. *Comput. Mater. Sci.* **2014**, *81*, 446−452.

(33) Perdew, J. P.; Burke, K.; Ernzerhof, M. Generalized Gradient Approximation Made Simple. *Phys. Rev. Lett.* **1996**, *77* (18), 3865−3868.

(34) Grimme, S.; Antony, J.; Ehrlich, S.; Krieg, H. A Consistent and Accurate Ab Initio Parametrization of Density Functional Dispersion Correction (DFT-D) for the 94 Elements H-Pu. *J. Chem. Phys.* **2010**, *132* (15), 154104.

(35) Liechtenstein, A. I.; Anisimov, V. I.; Zaanen, J. Density-Functional Theory and Strong Interactions: Orbital Ordering in Mott-Hubbard Insulators. *Phys. Rev. B: Condens. Matter Mater. Phys.* **1995**, *52* (8), R5467.

(36) Anisimov, V. I.; Zaanen, J.; Andersen, O. K. Band Theory and Mott Insulators: Hubbard U Instead of Stoner I. *Phys. Rev. B: Condens. Matter Mater. Phys.* **1991**, *44* (3), 943−954.

(37) Anisimov, V. I.; Solovyev, I. V.; Korotin, M. A.; Czyzyk, M. T.; Sawatzky, G. A. Density-Functional Theory and NiO Photoemission Spectra. *Phys. Rev. B: Condens. Matter Mater. Phys.* **1993**, *48* (23), 16929−16934.
(38) Kim, B. G.; Toyoda, M.; Park, J.; Oguchi, T. Electronic Structure and Phase Transition in Polar $ScFeO_3$ from First Principles Calculations. *J. Alloys Compd.* **2017**, *713*, 187−193.
(39) Holtz, M. E.; Shapovalov, K.; Mundy, J. A.; Chang, C. S.; Yan, Z.; Bourret, E.; Muller, D. A.; Meier, D.; Cano, A. Topological Defects in Hexagonal Manganites: Inner Structure and Emergent Electrostatics. *Nano Lett.* **2017**, *17*, 5883−5890.
(40) Lauritsen, J. V.; Jensen, M. C. R.; Venkataramani, K.; Hinnemann, B.; Helveg, S.; Clausen, B. S.; Besenbacher, F. Atomic-Scale Structure and Stability of the $\sqrt{31} \times \sqrt{31}$R9° Surface of Al_2O_3(0001). *Phys. Rev. Lett.* **2009**, *103* (7), No. 076103.
(41) Georgescu, A. B.; Ismail-Beigi, S. Surface Piezoelectricity of (0001) Sapphire. *Phys. Rev. Appl.* **2019**, *11*, No. 064065.
(42) Moetakef, P.; Ouellette, D. G.; Zhang, J. Y.; Cain, T. A.; Allen, S. J.; Stemmer, S. Growth and Properties of $GdTiO_3$ Films Prepared by Hybrid Molecular Beam Epitaxy. *J. Cryst. Growth* **2012**, *355*, 166.
(43) Lee, J. H.; Luo, G.; Tung, I. C.; Chang, S. H.; Luo, Z.; Malshe, M.; Gadre, M.; Bhattacharya, A.; Nakhmanson, S. M.; Eastman, J. A.; et al. Dynamic Layer Rearrangement during Growth of Layered Oxide Films by Molecular Beam Epitaxy. *Nat. Mater.* **2014**, *13* (9), 879−883.
(44) Jungbauer, M.; Hühn, S.; Egoavil, R.; Tan, H.; Verbeeck, J.; Van Tendeloo, G.; Moshnyaga, V. Atomic Layer Epitaxy of Ruddlesden−Popper $SrO(SrTiO_3)_n$ Films by Means of Metalorganic Aerosol Deposition. *Appl. Phys. Lett.* **2014**, *105* (25), 251603.
(45) Palgrave, R. G.; Borisov, P.; Dyer, M. S.; Mcmitchell, S. R. C.; Darling, G. R.; Claridge, J. B.; Batuk, M.; Tan, H.; Tian, H.; Verbeeck, J. Artificial Construction of the Layered Ruddlesden−Popper Manganite $La_2Sr_2Mn_3O_{10}$ by Reflection High Energy Electron Diffraction Monitored Pulsed Laser Deposition. *J. Am. Chem. Soc.* **2012**, *134*, 7700.

https://doi.org/10.1021/acs.chemmater.1c02079
Chem. Mater. 2021, 33, 7423−7431